Virial scaling of galaxies in clusters: bright to faint is cool to hot

Hao-Yi Wu,[1][*] Oliver Hahn,[2] August E. Evrard,[1] Risa H. Wechsler,[3] Klaus Dolag[4,5]

[1] *Department of Physics, University of Michigan, Ann Arbor, MI 48109, USA*
[2] *Department of Physics, ETH Zurich, CH-8093 Zürich, Switzerland*
[3] *KIPAC, Stanford University, SLAC National Accelerator Laboratory, Menlo Park, CA 94025, USA*
[4] *Universitätssternwarte, D-81679 München, Germany*
[5] *Max-Planck-Institut für Astrophysik, D-85748 Garching, Germany*

20 September 2013

ABSTRACT
By combining galaxy tracers from high-resolution N-body and hydrodynamical simulations, we present a consistent picture of the behaviour of galaxy velocities in massive clusters. In haloes above $\sim 10^{14} M_\odot$, the brightest satellite galaxies are slightly cooler compared to the dark matter, while fainter satellites are hotter. Within the virial radius of a cluster, the mean velocity dispersion based on the 100 brightest galaxies is a factor of $1.065 \pm 0.005\,(\mathrm{stat})\,\pm 0.027\,(\mathrm{sys})$ higher than that of the dark matter (corresponding to a $\sim 10 - 15$ per cent bias in the dynamical mass estimate) while that based on only the five brightest galaxies is $0.868 \pm 0.039\,(\mathrm{stat})\,\pm 0.035\,(\mathrm{sys})$. These trends are approximately independent of redshift. The velocity structure is sensitive to the modelling of galaxies in clusters, indicative of the complex interplay of tidal stripping, dynamical friction, and merging. Velocity dispersions derived from instantaneous subhalo properties are larger than those employing either peak subhalo properties or hydrodynamical galaxy tracers. The latter two methods are consistent, implying that stacked spectroscopic analysis of cluster samples should, after correction for projection, show a trend towards slightly higher velocities when fainter galaxies are included, with an unbiased measure of dark matter velocity dispersion coming from approximately 30 galaxies per cluster. We show evidence that the velocity distribution function of bright galaxies near the cluster centre has a low-velocity tail due to strong dynamical friction.

Key words: methods: numerical—galaxies: clusters: general—galaxies: haloes—cosmology: theory—dark matter.

1 INTRODUCTION

Dynamical measurements of galaxy cluster masses — based on the line-of-sight galaxy velocities from spectroscopic observations — have a long history, using a broad range of methods, including the direct application of the virial theorem (e.g., Yahil & Vidal 1977; Danese et al. 1980; Heisler et al. 1985; Girardi et al. 1993; Lubin & Bahcall 1993; Carlberg et al. 1997), the caustic method measuring the escape velocity of galaxies (e.g., Diaferio & Geller 1997; Diaferio 1999), and Jeans analysis (e.g, Łokas & Mamon 2003; Mamon et al. 2013). Recent cluster surveys have enabled new studies of the relation between velocity dispersion and other cluster mass proxies, including optical richness (e.g., Becker

et al. 2007, and Andreon & Hurn 2010 based on SDSS), Sunyaev-Zel'dovich effect (e.g., Rines et al. 2010 based on HeCS, and Sifón et al. 2013 based on ACT), and X-ray luminosity or temperature (e.g., Zhang et al. 2011 based on HIFLUGCS, and Rines et al. 2013 based on HeCS). With the current observational resources, most of these studies focus on a few tens of clusters with $\sim$100 member galaxies for each cluster, i.e., $\sim$10,000 spectra in total. These samples are often limited by statistics; upcoming deep, wide spectroscopic surveys such as *Euclid* (Laureijs et al. 2011), *Subaru* Prime Focus Spectrograph (Ellis et al. 2012), and BigBOSS[1] will allow more detailed study of how dynamical masses relate to other mass proxies.

On the theoretical side, the virial scaling relation be-

---

[*] E-mail: hywu@umich.edu

[1] http://bigboss.lbl.gov

tween halo mass and the velocity dispersion of *dark matter* (DM) has been established at high precision using simulation ensembles (Evrard et al. 2008). The dynamics of galaxies, however, may be different from that of the DM due to a number of physical processes, such as dynamical friction, tidal stripping and disruption, mergers, and hydrodynamic drag by the gas in the cluster. This "velocity bias" of galaxies with respect to DM has been explored with ever improving simulations and cluster galaxy models (e.g., Carlberg et al. 1990; Carlberg 1994; Evrard et al. 1994; Summers et al. 1995; Frenk et al. 1996; Ghigna et al. 2000; Colín et al. 2000; Gill et al. 2004; Gao et al. 2004; Diemand et al. 2004; Faltenbacher & Diemand 2006; Lau et al. 2010; Munari et al. 2013). However, discrepancies in the measured velocity bias exist among simulations with different numerical treatments and different galaxy tracers (see Section 3 for a review). A principal goal of this paper is to demonstrate the origin of these differences and to show that a consistent picture appears to be emerging when state-of-the-art galaxy tracers are used.

In this work, we focus on the velocity dispersion of galaxies in massive clusters, using the N-body simulation suite RHAPSODY and the hydrodynamical simulation MAGNETICUM PATHFINDER. We study the velocity bias using various galaxy tracers in both simulations and compare with results in the literature. Using the rich galaxy statistics from RHAPSODY, we quantify statistically the virial scaling relation obtained from different galaxy populations. We then compare the dynamical structure of galaxies in both simulations.

We note that the 3D effects presented in this work will be complicated by the projection effect in observations, which both increases scatter and introduces potential biases in cluster mass estimates (e.g., Biviano et al. 2006; Cohn et al. 2007; Wojtak et al. 2007; Mamon et al. 2010; White et al. 2010; Cohn 2012; Saro et al. 2013; Gifford & Miller 2013; Gifford et al. 2013). Here, we focus on quantifying the theoretical uncertainty in the *intrinsic* velocity structure of clusters in order to pave the way for future studies that incorporate observational complications.

This paper is organized as follows. Section 2 introduces the simulation data and the galaxy tracers used in this work. Section 3 compares the velocity bias results in this work and in the literature and presents a converging picture. Section 4 discusses the virial scaling calibrated from galaxies. In Section 5, we explore in detail the velocity structure of cluster galaxies to better understand the physical processes causing velocity bias. In Section 6, we compare the velocity structures in N-body and hydrodynamical simulations. We conclude in Section 7.

2   SIMULATIONS

In this work, we use a suite of zoom-in DM simulations of galaxy clusters called RHAPSODY and a cosmological box from the hydrodynamical simulation MAGNETICUM PATHFINDER. The simulation parameters are summarized in Table 1. Although these two sets of simulations are based on slightly different cosmological parameters (see below), we expect that the impact on our results is negligible because

Evrard et al. (2008) have demonstrated that the virial scaling is insensitive to cosmology.

2.1   Pure dark matter N-body simulation: Rhapsody

The RHAPSODY simulation (Wu et al. 2013a) is a statistical sample of high-resolution N-body re-simulations of galaxy clusters, designed for studying the scatter of the observable–mass relation, a property essential for precision cosmology. The main sample includes 96 haloes at $z = 0$ with virial masses lying in a narrow range, $\log_{10}M_{\mathrm{vir}} = 14.8 \pm 0.05$, re-simulated from a $1\,h^{-1}$Gpc volume. The mass resolution is $1.3 \times 10^8\,h^{-1}\mathrm{M_\odot}$ (equivalent to 8192^3 particles in this volume), and the gravitational softening length is $3.3\,h^{-1}$kpc. In addition to haloes at $z = 0$, we include 8142 most-massive progenitors of them at 85 discrete redshifts up to $z = 2$ to calibrate the viral scaling relation.

The RHAPSODY simulation is based on the MUSIC code (Hahn & Abel 2011) to generate the multi-scale initial condition, the public version of GADGET-2 (Springel 2005) to perform the gravitational evolution, the ROCKSTAR (Behroozi et al. 2013a) phase-space halo finder to identify haloes and subhaloes, and the gravitationally consistent merger tree code (Behroozi et al. 2013b) to track the evolution history for haloes and subhaloes. The key properties of the main haloes and subhaloes in this sample have been presented in Wu et al. (2013a) and Wu et al. (2013b), respectively.

The cosmological parameters used in RHAPSODY are based on a flat Λ cold dark matter cosmology: $\Omega_{\mathrm{M}} = 0.25$, $\Omega_{\mathrm{b}} = 0.04$, $h = 0.7$, $\sigma_8 = 0.8$, and $n_s = 1$.

2.2   Hydrodynamical simulation: Magneticum Pathfinder

The MAGNETICUM PATHFINDER[2] is a new suite of hydrodynamical simulations that aim for multi-wavelength studies of galaxy clusters (Dolag et al. in preparation). This work is based on Box 3 of that suite, a cosmological volume with a side length $128\,h^{-1}$Mpc and 2×576^3 particles. The mass of DM particles is $6.9 \times 10^8\,h^{-1}\mathrm{M_\odot}$, and the mass of SPH gas particles is $1.4 \times 10^8\,h^{-1}\mathrm{M_\odot}$. The gravitational softening length is $5\,h^{-1}$kpc. This work uses the 46 haloes with $M_{\mathrm{vir}} > 10^{14}\,h^{-1}\mathrm{M_\odot}$ in this volume.

MAGNETICUM PATHFINDER uses the smoothed particle magnetohydrodynamics code P-GADGET3 (XXL), which includes star formation and chemical enrichment, active galactic nuclei (AGN) feedback, thermal conduction, passive magnetic fields, and magnetic dissipation. The subhaloes and galaxies in this simulation are identified with L-SUBFIND, presented in Dolag et al. (2009). In brief, L-SUBFIND improves upon the original SUBFIND code (Springel et al. 2001) to apply to DM, stellar, and gas particles. It identifies friends-of-friends structures based on DM particles, associates star and gas particles to the nearest DM particles, and calculates the SPH kernel density for each species separately. The unbinding procedure takes into account the internal thermal energy of gas particles. The centres of subhaloes

---

Type	Name	Mass res. $(10^8 h^{-1} M_\odot)$	Force res. $(h^{-1}\text{kpc})$	N_{halo}	M_{halo} $(10^{14} h^{-1} M_\odot)$
N-body	RHAPSODY	1.3	3.3	96 $(z = 0)$	6.3 ± 0.48
				8142 $(0 \leqslant z \leqslant 2)$	2.85 ± 1.99
Hydro	MAGNETICUM PATHFINDER	6.9 (DM) 1.4 (gas)	5	46 $(z = 0)$	> 1

Table 1. Simulations used in this work.

Label	Proxy of
N-body-v_0	Subhalo mass in N-body sims
N-body-v_{pk}	Galaxy luminosity in N-body sims
Hydro-v_0	Subhalo mass in hydro sims
Hydro-M_{star}	Galaxy stellar mass in hydro sims

Table 2. Summary of galaxy tracer populations.

Tracer	b_{v} for $N = 5$	b_{v} for $N = 100$
N-body-v_0	1.018 ± 0.013	1.119 ± 0.005
N-body-v_{pk}	0.899 ± 0.012	1.038 ± 0.004
Hydro-v_0	0.975 ± 0.018	1.066 ± 0.007
Hydro-M_{star}	0.949 ± 0.017	1.057 ± 0.006
Random	0.978	0.999

Table 3. Mean velocity bias of different galaxy tracer populations.

are chosen to be at the local minimum of the gravitational potential.

The cosmological parameters used in MAGNETICUM PATHFINDER are based on *Wilkinson Microwave Anisotropy Probe* 7 (Komatsu et al. 2011): $\Omega_{\text{M}} = 0.272$, $\Omega_{\text{b}} = 0.0456$, $\Omega_\Lambda = 0.728$, $h = 0.704$, $\sigma_8 = 0.809$, and $n_s = 0.963$.

2.3 Galaxy tracers in simulations

We consider a rank-ordered list of subhaloes in a halo as a proxy for a rank-ordered list of cluster galaxies. For the RHAPSODY simulation, subhaloes are ranked by their maximum circular velocity of DM, $v_{\text{max}} = \max[\sqrt{GM(< r)/r}]$, at two different epochs: an instantaneous value, v_0, which denotes the value of v_{max} evaluated at $z = 0$; v_{pk}, the peak value of v_{max} over its prior history. Ranking subhaloes by v_{pk} is known to be superior to v_0 ranking when comparing to mass- or luminosity- selected samples of galaxies; for example, recent analysis by Reddick et al. (2013) has shown that the v_{pk} prescription reproduces observed galaxy clustering in the local Universe with remarkable fidelity (also see, e.g., Nagai & Kravtsov 2005; Conroy et al. 2006; Wetzel et al. 2013).

For the MAGNETICUM PATHFINDER simulation, we employ both v_0 (derived from all mass components) and the stellar mass in subhaloes at $z = 0$ for ranking galaxies. Because cooling and star formation creates a more core-dominated subhalo structure in hydrodynamical simulations, we will see that using v_0 in MAGNETICUM PATHFINDER produces results consistent with those using the stellar mass, and also consistent with those using v_{pk} in RHAPSODY.

Our notation and a summary of these galaxy tracers are given in Table 2.

3 VELOCITY BIAS: A CONVERGING PICTURE

The 3D velocity dispersion of a group of N objects (DM particles or galaxies) in a system can be defined as

$$\sigma^2 = \frac{1}{N - 1} \sum_{i=1}^{N} ||\boldsymbol{v}_i - \bar{\boldsymbol{v}}||^2 \,, \tag{1}$$

where $\boldsymbol{v}_i$ denotes the 3D velocity of the ith object, and $\bar{\boldsymbol{v}}$ denotes the mean velocity of these N objects.

This difference between the velocity dispersion of galaxies (σ_{gal}) and that of DM (σ_{DM}) can be quantified by *velocity bias*, defined as:

$$b_{\text{v}} = \frac{\sigma_{\text{gal}}}{\sigma_{\text{DM}}} \,. \tag{2}$$

When we calculate σ_{DM}, we use all particles within R_{vir} around the central halo, which also corresponds to the brightest cluster galaxy (BCG) in our modelling. When we calculate σ_{gal}, we use all galaxies *except for the BCG* within R_{vir}. Here R_{vir} is the radius encompassing the overdensity Δ_{vir} calculated from a spherical collapse model (Gunn & Gott 1972). We employ the fitting function of Bryan & Norman (1998).

In each calculation, $\bar{\boldsymbol{v}}$ corresponds to the mean velocity of the particular population in question rather than the bulk velocity of the halo or the velocity of the BCG. This choice gives the minimal velocity dispersion and is presumably the closest to reality.

3.1 Velocity bias of different galaxy tracers

Fig. 1 compares our results of velocity bias (left-hand panel) with results from the literature (right-hand panel). Let us first focus on the left-hand panel, which presents b_{v} as a function of N, the number of brightest galaxies or most massive subhaloes used to measure σ_{gal}. The red/orange curve corresponds to N-body-v_0/N-body-v_{pk}, while the green/blue curve corresponds to Hydro-v_0/Hydro-M_{star}. We present the mean b_{v} of the $z = 0$ sample and the error on the mean. The
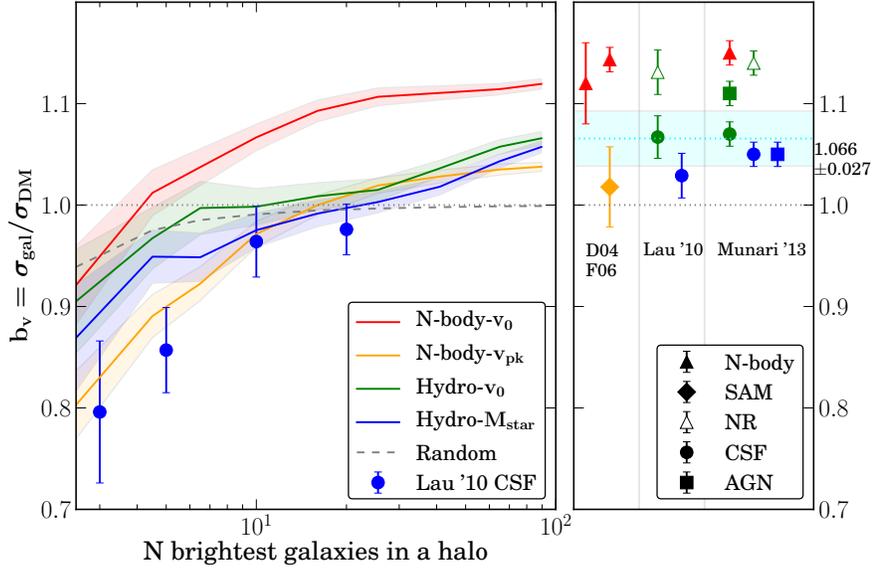
Figure 1. Velocity bias based on various simulations and galaxy tracers. The curves are the results of this work, showing how velocity bias depends on the number of brightest galaxies used to estimate the velocity dispersion. Subhaloes in N-body simulations (red) show substantial velocity bias, while galaxies modelled from N-body and hydro simulations (orange and blue) have a smaller velocity bias. Using v_{pk} as a luminosity proxy in the N-body simulation gives similar results as using v_0 and M_{star} in the hydro simulation.

grey dashed curve corresponds to selecting N random DM particles for measuring the velocity dispersion, reflecting the bias inherent to measuring σ with finite N.

When the number of galaxies is low, the velocity bias is less than 1 and slightly below the value expected from randomly sampled particles (although N-body-v_0 and Hydro-v_0 are consistent with the random case). This indicates that the brightest galaxies tend to be slower than DM particles and suggests a strong influence of dynamical friction (see e.g. Goto 2005 for observational evidence). On the other hand, when the number of galaxies is high, the velocity bias becomes greater than 1. This can be explained by the inclusion of fainter galaxies/low-mass subhaloes into the sample. The slow faint galaxies tend to be tidally disrupted or merge with the BCG, so that the surviving galaxies tend to be a fast population, thus biasing the velocity dispersion. We will further investigate how velocity bias depends on galaxy luminosity in Section 5.

We note that using N-body-v_0 tends to overestimate b_v, indicating that by using v_0 the sample of kinematic tracers becomes biased since strongly stripped, early accreted subhaloes drop out of the sample. These drop-outs tend to be slow, thus the velocity dispersion is increased. Comparing v_0 in both cases, we note that Hydro-v_0 has lower velocity bias, indicating that subhaloes are less prone to stripping and disruption in the hydro simulation than in the DM simulation. In fact, Hydro-v_0 behaves more similar to N-body-v_{pk} at high N. Although the clusters in N-body and hydro simulations have different masses (as indicated in Table 1), we note that the results here are roughly independent of halo mass and redshift, which will be shown in Fig. 2. In Table 3, we compare b_v from these four galaxy/subhalo populations.

3.2 Comparison with the results in the literature

The right-hand panel of Fig. 1 shows the comparison between our results and the following results from the literature: (1) Diemand et al. (2004, D04) and Faltenbacher & Diemand (2006, F06); (2) Lau et al. (2010); and (3) Munari et al. (2013). These results are representative of the diversity of the predictions from different simulations, which can usually be put into one of these four categories.

(i) *Subhaloes from dark matter N-body simulations* (marked as red). The velocities of "resolved" subhaloes are used to compute the velocity dispersion, and subhaloes are selected based on their current mass or v_0 (like our N-body-v_0). These samples show $b_v > 1$, but the value of b_v depends on the resolution of the simulation and the criterion of subhalo selection (e.g., Colín et al. 2000; Diemand et al. 2004; Faltenbacher & Diemand 2006). Increasing the resolution tends to reduce the velocity bias, indicating that the positive velocity bias can be a result of over-merging, which tends to remove slow and less massive subhaloes.

(ii) *Galaxies inferred from dark matter N-body simulations* (marked as orange). There are two common methods to predict the galaxy properties from DM N-body simulations. The first method is entirely based on resolved subhaloes and assigning galaxy luminosity based on the subhalo mass before accretion (like our N-body-v_{pk}). We find that N-body-v_{pk} leads to smaller b_v than N-body-v_0, indicating that the most massive subhaloes and the brightest galaxies in a cluster are two populations with different dynamical properties. The former population tends to exclude the highly stripped subhaloes, which have been accreted early and have slow velocities, and include the recently accreted subhaloes, which still have high v_0 and high orbital velocities (e.g., Gao et al. 2004). The second method is to apply

semi-analytic models (SAMs) for galaxy formation and to track galaxies using their "most-bound particles" after their subhaloes are disrupted. In this case, b_v is greatly reduced because a fraction of the galaxies, by construction, have the same velocities as DM particles. For example, Faltenbacher & Diemand (2006) have found such a trend between their two samples based on subhaloes and most-bound particles (red and orange triangles; also see, e.g., Gao et al. 2004; Faltenbacher et al. 2005; Sales et al. 2007). While using this method, one should caution that SAMs do not always reproduce the observed galaxy number density profile at small radii (e.g., Budzynski et al. 2012).

(iii) *Subhaloes in hydrodynamical simulations* (marked as green). This is mainly used to compare with category (i) to illustrate the impact of baryonic physics. We use resolved subhaloes in the hydro simulation based on the mass proxy v_0 (Hydro-v_0), and its b_v is lower than N-body-v_0 but similar to N-body-v_{pk}. This indicates that subhaloes in the hydro simulation are more resistant to stripping than their counterparts in N-body simulations, because of the star particles condensed in the centre of subhaloes. This result also implies that v_0 in the hydro simulation behaves similar to v_{pk} in the DM simulation. However, simulations with different baryonic physics have reported various values. In the right-hand panel, we show various results from Lau et al. (2010) and Munari et al. (2013), which includes simulations with "NR" (non-radiative, open triangles), "CSF" (cooling and star formation, circles), and "AGN" (feedback from active galactic nuclei, squares). In general, "NR" processes tend to give results very similar to pure DM simulations because these simulations tend to produce puffy subhaloes which are prone to stripping; "CSF" can reduce the velocity bias because it can produce stellar cores; "AGN" again brings up velocity bias because the core density is reduced. The results could still vary based on the implementation of the feedback. We note that these different feedback processes can also alter the density profile of the main halo and thus σ_{DM}; for example, CSF tends to generate a high-density stellar core, while AGN tends to reduce the core density (e.g., Dubois et al. 2011; Martizzi et al. 2012).

(iv) *Galaxies in hydrodynamical simulations* (marked as blue). Hydrodynamical simulations with star formation prescriptions can directly predict the properties of galaxies. These galaxies have been consistently shown to have very small velocity bias. We note that b_v from Hydro-M_{star} is slightly smaller than that of Hydro-v_0. We also show results from Lau et al. (2010, CSF) and Munari et al. (2013, CSF and AGN) as blue points. However, it is still computationally prohibitive to generate a statistical sample of high-resolution cluster galaxies with an adequate span of the range of plausible recipes for baryonic physics to minimize both the statistical and systematic errors.

Fig. 1 shows a converging picture for the velocity bias obtained from simulations based on different techniques. Combing our measurements from N-body-v_{pk}, Hydro-v_0, and Hydro-M_{star}, as well as the b_v values from SAM, CSF, and AGN in the literature [i.e. the orange, blue, and green points (excluding NR) and curves, from which we take the value at high N] leads to $1.065 \pm 0.005 \,(\text{stat}) \pm 0.027 \,(\text{sys})$, where the statistical error is the error on the weighted mean, while the systematic error is the weighted sample variance
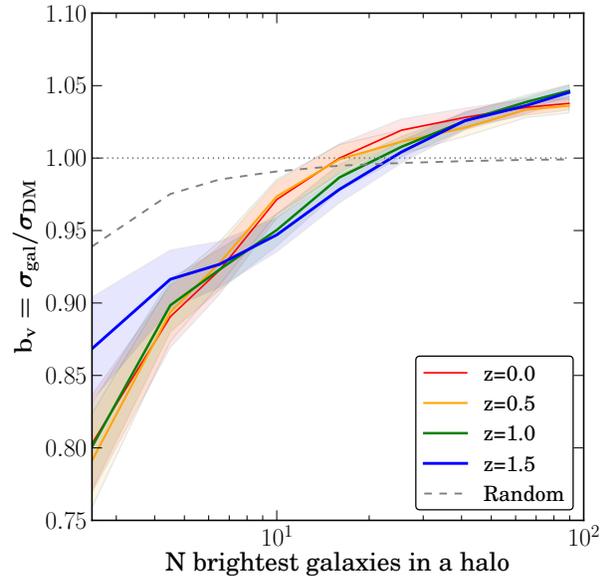

Figure 2. Velocity bias of galaxies selected by v_{pk} in the DM simulation, for $z = 0$, 0.5, 1, and 1.5. For high N, the velocity bias is consistent with no evolution. For low N, low-redshift bright galaxies are slightly slower than high-redshift ones, indicating that the dynamical friction has been lasting for a longer time.

among different measurements. The same calculation for $N = 5$ gives $0.868 \pm 0.039 \,(\text{stat}) \pm 0.035 \,(\text{sys})$.

While we were finalizing this manuscript we learned of the related work by Old et al. (2013). They use a semi-analytic treatment to trace galaxies and find values of b_v below unity at the bright end that are consistent with our findings. They also see b_v increasing for faint galaxies, but do not find values b_v above unity. There are subtle differences between their analysis methods and ours which may be driving the faint-end differences. We note that: (1) the hydrodynamical simulations used here, which one can argue are the most realistic of the methods under discussion, show $b_v = 1.06$ at $N = 100$, and (2) taking a conservative sum of our systematic and statistical errors our findings are consistent with b_v of unity at the $\sim 2\sigma$ level.

3.3 Redshift evolution

Fig. 2 shows the velocity bias at four different redshifts from the RHAPSODY simulation, using v_{pk} as a luminosity proxy, as a function of the number of brightest galaxies used. For high N, the results are independent of redshift. For low N, b_v has a slight trend with redshift; the brightest galaxies at low redshift tend to be slower than those at high redshift. This is plausibly explained by the effect of dynamical friction. Since haloes at different redshifts also have different masses, our finding here implies that this relation is independent of mass. We have explicitly verified this statement.

Munari et al. (2013) have shown that the velocity bias decreases at high redshift, which is in apparent disagreement with our findings. This difference could result from the different galaxy population we use; while we compare
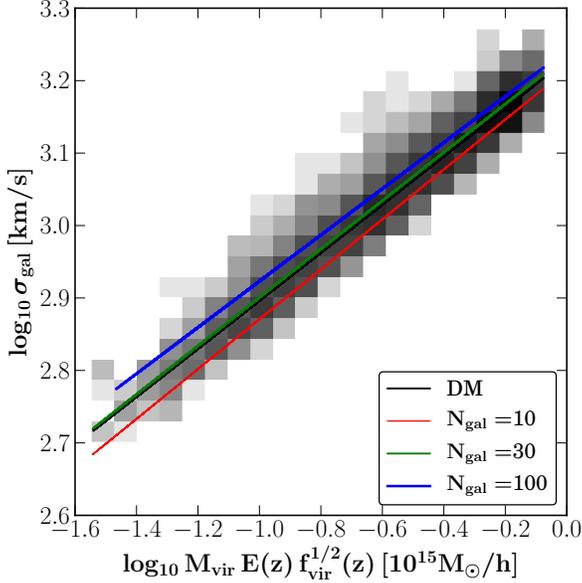
Figure 3. The virial scaling relation calibrated using galaxies and DM particles in RHAPSODY. The grey 2D histogram corresponds to measurements from the DM particles, and the best-fitting relation agrees with Evrard et al. (2008). The three colour curves represent the fit of the virial scaling relation using the 10/30/100 brightest galaxies in each halo, and the values of fitting parameters are given in Table 4. When we use the 10 brightest galaxies (red curve), the normalization is lower by $\approx 3\%$. On the other hand, with 100 galaxies, the normalization is higher by $\approx 3\%$.

$N_{\rm gal}$	$\sigma_{\rm gal,15}$	α	$\sqrt{\langle \delta^2_{\ln \sigma} \rangle}$	shot noise
10	1641±32	0.34±0.01	0.142	0.134
30	1716±33	0.33±0.01	0.092	0.073
100	1746±34	0.32±0.01	0.072	0.039
DM	1692±33	0.33±0.01	0.053	NA

Table 4. Fitting parameters in Fig. 3. The scatter of each fit agrees with the intrinsic scatter combined with the shot noise.

the same number of galaxies per halo across all redshifts, Munari et al. (2013) set constant thresholds for the dark mass of subhaloes ($10^9 {\rm M}_\odot$) and the stellar mass of galaxies ($3 \times 10^9 {\rm M}_\odot$) across all redshifts. This constant threshold will lead to fewer galaxies per cluster at high redshift. Since fewer galaxies can results in lower $b_{\rm v}$, this constant threshold can result in a smaller $b_{\rm v}$ at high redshift.

4 VIRIAL SCALING FROM CLUSTER GALAXIES

Fig. 3 presents the virial scaling between cluster mass and $\sigma_{\rm gal}$ measured with 10/30/100 brightest galaxies (red/green/blue), compared with $\sigma_{\rm DM}$ (black). We use 85 time steps between $z = 0$ and 2 from the RHAPSODY simulation and use $v_{\rm pk}$ as the luminosity proxy, assuming that different evolutionary stages of the same haloes can pro-

vide a fair sample of the dynamical states. We justify this assumption by examining whether the virial scaling ($\sigma_{\rm DM}$–$M_{\rm vir}$ relation) of this sample agrees with previous results from the volume-limited sample of Evrard et al. (2008). The grey-scale is a 2D histogram of $\sigma_{\rm DM}$ and $M_{\rm vir}$ of these haloes, whose virial masses are scaled with the Hubble parameter $E(z) = h(z)/h_0$ and the square root of the virial overdensity $f_{\rm vir} = \Delta_{\rm vir}(z)/\Delta_{\rm vir}(z = 0)$, for the purpose of eliminating the effect of the evolution of the background density and the virial overdensity. These haloes follow the scaling relation

$$\ln \sigma_{\rm DM} = \ln \left[1692.17 \, {\rm km \, s}^{-1} \right] + 0.33 \ln \left[M_{\rm vir} E(z) f_{\rm vir}^{1/2}(z) \right] \tag{3}$$

with a scatter

$$\langle \delta^2_{\ln \sigma} \rangle^{1/2} = \left\langle (\ln \sigma - \ln \sigma_{\rm fit})^2 \right\rangle^{1/2} = 0.05 \tag{4}$$

These values agree with those quoted in Evrard et al. (2008) (see their table 6; normalization $982\sqrt{3} = 1700$, slope 0.355, and scatter 0.0527), indicating that using multiple snapshots for each halo can provide a fair sample of the dynamical state of haloes.[3]

We now compare the virial scaling measured from different galaxy samples. The colour lines show the best-fitting linear relation, and Table 4 lists the best-fitting parameters of the following parametrization:

$$\ln \sigma_{\rm gal} = \ln \sigma_{\rm gal,15} + \alpha \ln \left[M_{\rm vir} E(z) f_{\rm vir}^{1/2}(z) \right] \tag{5}$$

Using the 10 brightest galaxies to calibrate the scaling relation biases the normalization low by $\approx 3\%$. When we use the 30 brightest galaxies, the normalization agrees almost perfectly with the results using DM particles. When we increase the number to 100, the normalization is higher by $\approx 3\%$. This trend of normalization with galaxy number agrees with the trend of velocity bias presented in Fig. 1.

We note that these different selections of galaxies tend to give the same slope as using DM particles, ≈ 0.33. This result is contrary to the findings of Munari et al. (2013), who have found a slope of ≈ 0.36 for the virial scaling from subhaloes and galaxies. Again, this discrepancy could result from the different subhalo/galaxy population we use. While we use a constant number of galaxies per cluster, Munari et al. (2013) set constant mass thresholds for subhaloes and galaxies. For less massive haloes, galaxies above these thresholds are rare and relatively massive compared with the host halo; thus, these galaxies are prone to the effect of dynamical friction and become slower. Therefore, a constant galaxy mass threshold can cause $b_{\rm v} < 1$ for less massive haloes, thus leading to a steeper slope.

Finally, we compare the scatter, $\langle \delta^2_{\ln \sigma} \rangle^{1/2}$, of each fit. We have shown above that the virial scaling based on DMr particles presents a 5% intrinsic scatter. If we choose a small number of galaxies $N_{\rm gal}$ to calculate the velocity dispersion, there is an additional statistical error ("shot noise"), presented in the last column of Table 3. We note that for the $N_{\rm gal}$ we considered here (10/30/100), the total scatter (0.14/0.09/0.07) is consistent with the combination of intrinsic scatter (0.05) and shot noise (0.13/0.073/0.040). Our

---

[3] Recently, Diemer et al. (2013) have shown that this virial scaling relation is robust regardless of the accretion rate, indicating that haloes tend to be in local Jeans equilibrium.
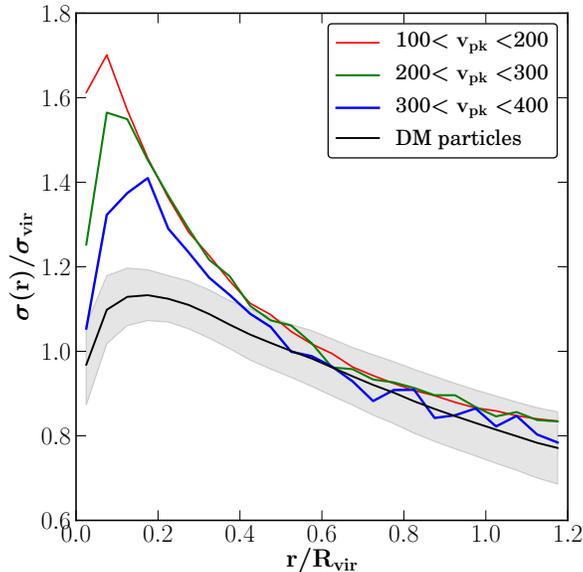
Figure 4. Velocity dispersion profile for DM (black curve) and cluster galaxies (colour curves) in RHAPSODY. Galaxies are binned by the luminosity proxy v_{pk}. Galaxies in all three bins have higher velocity dispersion than DM particles within $0.5R_{vir}$. The red curve, which corresponds to the faintest galaxies, has the highest velocity bias.
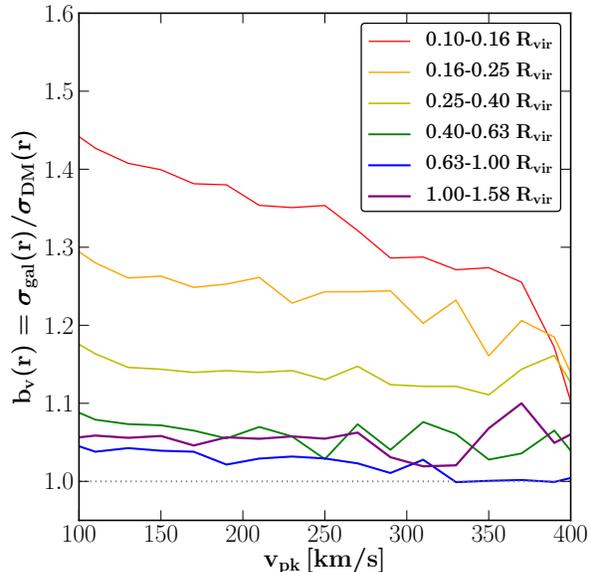
Figure 5. Velocity bias for galaxies in RHAPSODY as a function of luminosity proxy v_{pk}, binned by radius (different curves). Galaxies in the inner region of clusters (red and orange) tend to have the highest velocity bias, which can be caused by strong tidal stripping and disruption in this region. Brighter galaxies (larger v_{pk} values) tend to be slower due to dynamical friction.

values also bracket the values quoted in Munari et al. (2013) (their fig. 6).

We note that a 3% bias in velocity dispersion corresponds to a 9% bias in dynamical mass, which can be a dangerous source of systematic error if one uses spectroscopic follow-up for mass calibration for photometric cluster surveys (e.g., Wu et al. 2010). In addition, an accurate calibration of the scatter of the mass–observable distribution is essential for accounting for the Eddington/Malmquist bias of the cluster abundance and for interpreting the observed massive, distant clusters (e.g., Mortonson et al. 2011).

5 VELOCITY STRUCTURE OF CLUSTER GALAXIES

5.1 Dependence of velocity bias on radius and luminosity: a stacking analysis

Two major physical processes that can produce velocity bias in collisionless systems are dynamical friction and tidal disruption. Dynamical friction tends to slow down galaxies and make them approach $b_v \sim 1$ (e.g., Boylan-Kolchin et al. 2008). Tidal disruption tends to occur in high density regions and remove slow galaxies (e.g., Wetzel & White 2010), thus increasing velocity bias. We would like to disentangle these processes by examining the velocity bias as a function of galaxy luminosity and the distance to the cluster centre. To this end, we use the rich statistics of cluster galaxies in RHAPSODY to study their velocity structures, focusing on how the galaxy velocity depends on luminosity (modelled by v_{pk}) and its distance to cluster center. We use 32 outputs between $0 \leqslant z \leqslant 0.5$ and assume that the relation between

luminosity and v_{pk} has negligible evolution in this redshift range.

Our stacking process is as follows. For a galaxy with velocity $\boldsymbol{v}_{gal}$ in a halo of velocity dispersion σ_{vir}, we define

$$\boldsymbol{v}' = \frac{\boldsymbol{v}_{gal} - \boldsymbol{v}_{cen}}{\sigma_{vir}} \;, \qquad (6)$$

where $\boldsymbol{v}_{cen}$ is the velocity of the BCG, and σ_{vir} is the DM velocity dispersion of the host halo. The stacked velocity bias is given by

$$b_{v,\,stack}^2 = \frac{1}{N-1} \sum_{i=1}^{N} ||\boldsymbol{v}'_i - \bar{\boldsymbol{v}}'||^2 \;, \qquad (7)$$

where N is the number of galaxies, and $\bar{\boldsymbol{v}}'$ is the mean of $\boldsymbol{v}'$ in this stack of galaxies. This is analogous to Equation 1 but takes into account the different masses of host haloes by dividing galaxy velocities by σ_{vir}. Under this definition, the stacked velocity bias is the dispersion of velocity ratio, rather than the ratio of velocity dispersion.

Fig. 4 presents the stacked velocity bias profile of galaxies, binned by the luminosity proxy v_{pk} (colour curves). The velocity dispersion profile of DM is presented as the black curve. Beyond $0.5R_{vir}$, galaxy velocity is roughly unbiased. The brightest galaxies (blue) has slightly lower velocity bias, indicating that the effect of dynamical friction is stronger for brighter/more massive galaxies. On the other hand, at smaller radii, the faintest sample (red) shows the largest velocity bias, while the brightest sample shows the least velocity bias. This can be explained by the tidal disruption of faint galaxies, which is stronger at smaller radii, where the density is high. We note that Ludlow et al. (2009) have shown that in Milky Way-size haloes, the radial velocity dispersion
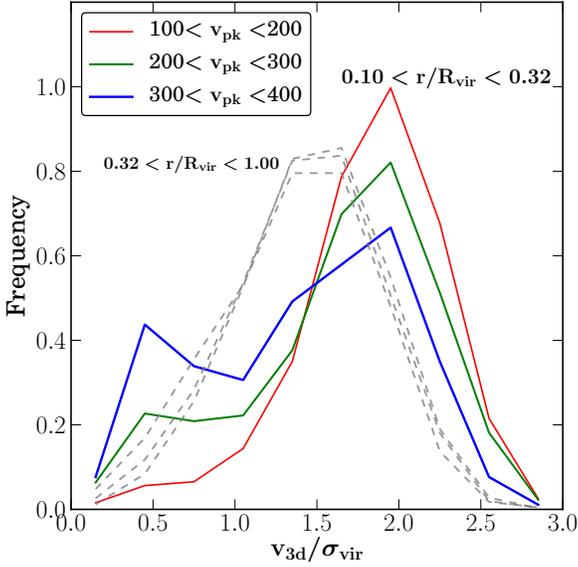
Figure 6. The velocity distribution function for different galaxy populations. Here we highlight $0.1 < r/R_{\rm vir} < 0.32$, and different colour curves present different luminosity bins (modelled by $v_{\rm pk}$). Bright galaxies have a highly negatively-skewed VDF, with a heavy tail of slow galaxies. This trend indicates that the velocity dispersion inferred from bright galaxies near the cluster centre tend to be lower. We note that this trend is largely diminished at larger radii (grey dashed curves correspond to $0.32 < r/R_{\rm vir} < 1$).

profile of subhaloes depends on subhalo mass; low-mass subhaloes have higher velocity bias than high-mass subhaloes. This trend is consistent with our findings.

Fig. 5 shows another aspect of the radial and luminosity dependence of velocity bias. Galaxies are put into logarithmically spaced radial bins (5 bins per decade), as indicated by the legend. To focus on the *local* velocity bias, in the stacking process, galaxies in a radial bin are compared with the DM in the same radial bin; that is,

$$\boldsymbol{v}'(r) = \frac{\boldsymbol{v}_{\rm gal} - \boldsymbol{v}_{\rm cen}}{\sigma_{\rm DM}(r)} \qquad (8)$$

The x-axis indicates the luminosity proxy $v_{\rm pk}$, while the y-axis indicates the stacked velocity bias in for a given radial bin.

For faint galaxies (low $v_{\rm pk}$), the inner radial bins (red, orange, and yellow) show significant velocity bias with a clear trend with radius. At small radii, faint galaxies experience stronger tidal stripping and are more easily disrupted, and the surviving subhaloes tend to be the fast ones and have high velocity bias. In addition, bright galaxies (high $v_{\rm pk}$) tend to be slower than faint galaxies because they have been slowed down more by dynamical friction. At large radii, the dependence on luminosity is weak, because galaxies are still infalling and have not experienced dynamical friction for long.

5.2 Velocity distribution function of cluster galaxies

In addition to the velocity dispersion, we would like to quantify the full velocity distribution function (VDF) of cluster galaxies to improve our understanding of the velocity structure of different galaxy populations. Fig. 6 presents the VDF of cluster galaxies from stacking the RHAPSODY sample ($0 \leqslant z \leqslant 0.5$), using $\boldsymbol{v}'$ as the scaled velocity of each galaxy. Galaxies are binned by the luminosity proxy $v_{\rm pk}$.

We have found that most radial ranges give very similar VDFs (an example is shown by the grey dashed curves), except for the radial range of $0.1 < r/R_{\rm vir} < 0.32$ (colour curves). At this radial range, bright galaxies show a highly negatively-skewed VDF, with the presence of a slow population, reflecting the strong effect of dynamical friction in this regime. We note that this VDF tail is not caused by the BCG, which is excluded in this analysis. This trend does not exist at larger radii; for comparison, the grey cash curves show the radial range of $0.32 < r/R_{\rm vir} < 1$, where different luminosity bins show similar VDFs.

Although this slow and luminous galaxy population is identified using galaxy tracers in N-body simulations, we note that this population also exists in hydro simulations, in which gas can further slow down these galaxies. This prediction is also robust with increased resolution, because this galaxy population corresponds to well-resolved subhaloes in the current simulation.

Finally, we caution that this slow population could potentially bias the dynamical mass measurements. When following up a cluster using spectroscopy, one tends to start from the brightest galaxies closest to the centre to reduce the impact of interlopers. Our results indicate that this strategy could bias the dynamical mass low. In addition to cluster mass calibration, we note that the VDF is also an important input in the Jeans analysis (e.g., Mamon et al. 2013) and in the modelling of redshift-space distortions of small-scale galaxy clustering (e.g., Tinker 2007). Therefore, an accurate characterization of the cluster galaxy VDF is essential for both cluster counting and galaxy clustering experiments.

6 COMPARING DARK MATTER AND HYDRODYNAMICAL SIMULATIONS

In this section, we discuss how the velocity structure of cluster galaxies could be altered by baryonic physics. We compare the DM simulation RHAPSODY ($z = 0$ sample) with the hydro simulation MAGNETICUM PATHFINDER introduced in Section 2 in Table 1.

Fig. 7 compares the velocity dispersion profile of galaxies and DM particles in the N-body (red) and hydro (blue) simulations. Let us first compare the DM particles (dotted curves). In the N-body simulation, the velocity dispersion decreases towards the centre, which is expected from the Navarro–Frenk–White (NFW) profile and is consistent with results from previous N-body simulations (e.g., Cole & Lacey 1996; Colín et al. 2000; Navarro et al. 2010). On the other hand, in the hydro simulation, the velocity dispersion stays nearly constant towards the center. This flat velocity dispersion profile has also been seen in the BCGs in the MAGNETICUM PATHFINDER simulation, as well as for elliptical galaxies in several hydro simulations, in Remus et al.
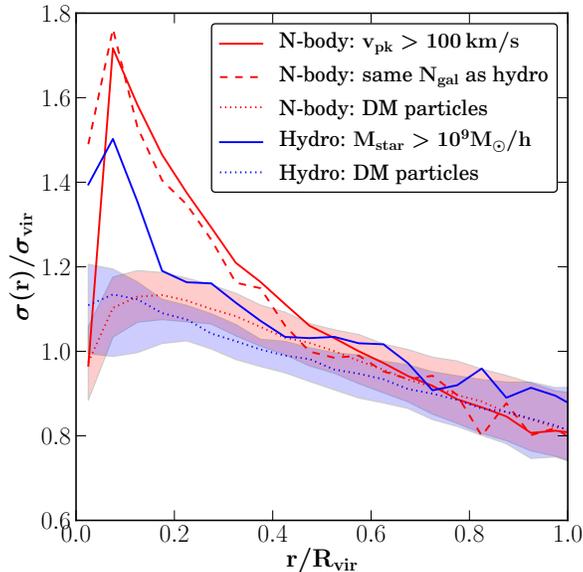
Figure 7. Velocity dispersion profile of haloes from the *N*-body simulation (red) and the hydro simulation (blue) at $z = 0$. Dark matter particles in the hydro simulation tend to be faster at small radii (dotted curves). We note that this difference cannot be accounted for by the mass differences in these two samples. On the other hand, galaxies in the hydro simulation tend to be slower (solid curves). Overall, galaxies in the hydro simulation have smaller velocity bias in the inner regions than those in the *N*-body simulation.

(2013). Possible explanations of this difference include (1) change in the density profile, and (2) change in the kinematics with the implementation of baryonic physics. When we investigate the density profile, we find that the hydro simulation does not produce an artificial high-density core (which has been seen in CSF simulations), because the simulation includes the AGN feedback and avoids the overcooling problem (see e.g., Teyssier et al. 2011; Martizzi et al. 2012 on the effect of AGN feedback on the density profile). Newman et al. (2013) have also shown that hydro simulations with AGN feedback can reproduce the observed cluster density profiles better than those without. Therefore, the near-isothermal core is not due to a significant deviation of density in the core. On the other hand, the AGN feedback may increase the kinetic energy of the DM particles near the cluster centre and make it close to isothermal. Early work without AGN feedback does not show such a nearly isothermal velocity dispersion profile (see e.g. Rasia et al. 2004 for non-radiative hydrodynamical simulations). This clearly presents a question that deserves further investigation in the future.

We now turn to the comparison of the velocity dispersion of cluster galaxies. The blue solid curve corresponds to galaxies in the hydro simulation with $M_{\mathrm{star}} > 10^9 h^{-1} \mathrm{M_\odot}$, and the red solid curve corresponds to galaxies in the *N*-body simulation with $v_{\mathrm{pk}} > 100 \, \mathrm{km \, s^{-1}}$; this choice is based on abundance matching between v_{pk} and M_{star} using cosmological simulations (Behroozi, private communication). To avoid the effect of the different galaxy number density pro-

files between the *N*-body and hydro simulations, we add another selection in the *N*-body simulation: the red dashed curve corresponds to selecting the same number of galaxies as in the hydro simulation at each radius. At smaller radii ($r < 0.5 R_{\mathrm{vir}}$), galaxies in the DM simulation tend to be faster than those in the hydro simulation, which can be attributed to stronger tidal disruption in *N*-body simulations. In addition, faint galaxies are dominant in number in our sample and are more susceptible to tidal disruption. Interestingly, in the innermost region ($r < 0.1 R_{\mathrm{vir}}$), the hydro simulation has faster DM particles but slower subhaloes compared with the *N*-body simulation in this region. We note that the shaded region indicates the halo-to-halo scatter (68 per cent interval). Although the scatter is large, the mean is robustly determined given our sample size. Therefore, the difference in the mean is significant.

We can see that the velocity bias is smaller in hydro simulations, i.e., the velocity of galaxies follow that of DM more closely. This can be attributed to two effects. First, in hydro simulations, the gas can exert a dragging force on to the galaxies that slows them down (e.g., Puchwein et al. 2005). Secondly, in hydro simulations, the cores of subhaloes are denser because of cooling and subsequent star formation in the center; therefore, these subhaloes tend to survive longer than those in pure DM simulations. These longer-lived subhaloes are also the slow population, which contributes to an overall lower velocity dispersion.

The second effect discussed above is related to the issue that subhaloes in pure DM simulations are often incomplete due to "over-merging" when compared with subhaloes in hydrodynamical simulations with star formation (e.g., Klypin et al. 1999; Weinberg et al. 2008; Dolag et al. 2009). In semi-analytic galaxy formation models, galaxies can be traced after subhalos disappear, either due to this over-merging effect or just due to the finite resolution; these are generally known as "orphan galaxies" (e.g., Gao et al. 2004). Whether this over-merging problem has been completely resolved by either hydro simulations or SAMs is still an open question. Future implementations of hydro simulations and galaxy tracer models will need to be critically compared with and constrained by observations, including the observed satellite content and radial profiles of galaxies in groups and clusters (e.g., Budzynski et al. 2012; Tinker et al. 2012; Newman et al. 2013; Reddick et al. 2013).

7 SUMMARY

Using *N*-body and hydrodynamical simulations of galaxy clusters, we have studied the velocity bias of different galaxy tracers and the virial scaling calibrated from galaxies. In particular, we have used the rich statistics of subhaloes in the RHAPSODY *N*-body simulation in parallel with galaxies identified in the MAGNETICUM PATHFINDER hydrodynamical simulation to study the velocity structure of cluster galaxies. Our findings can be summarized as follows.

• Galaxy populations inferred from either *N*-body simulations with v_{pk} as a luminosity proxy or hydrodynamical simulations show that the brightest cluster galaxies tend to underestimate, and faint galaxies slightly overestimate, the DM velocity dispersion. Our results indicate that selecting

$\sim$ 30 brightest cluster galaxies provide an approximately unbiased velocity dispersion.

• Ranking subhaloes by their instantaneous circular velocity, v_0, in N-body simulations leads to a larger velocity bias incompatible with the other galaxy tracers. We demonstrate consistency of our results with results in the literature that employ different tracer methods.

• Velocity bias tends to be higher for fainter galaxies at smaller cluster radii, indicating the stronger effect of tidal disruption, which removes slow galaxies efficiently in high density regions. Brighter galaxies are in general cooler, and we have identified that the brightest galaxies near the centre of a cluster (not the BCG) present a particularly slow population, which is plausibly consistent with dynamical friction.

• Comparing the hydrodynamical and N-body simulations, we have found that galaxy tracers in the former are less kinematically biased with respect to the DM. At small cluster radii, the DM in the hydro simulation has higher velocity dispersion than that in the N-body simulation, while the galaxies in the hydro simulations have *lower* velocity dispersion.

Current and near-future observed cluster samples with dense spectroscopy will be able to test for the differential effect from bright to faint magnitudes expected from simulations. Stacked sample analysis, such as has been done recently by Skielboe et al. (2012) to detect spatial velocity anisotropy, offers an attractive method to boost signal-to-noise ratio.

We remark that understanding the *intrinsic* dynamical properties of simulated galaxy tracers is important for using simulations to study observational complications such as projection effects and member galaxy selection (e.g., Gifford & Miller 2013; Gifford et al. 2013; Saro et al. 2013). In addition, the velocities of galaxies are essential for modelling the small-scale redshift-space distortions in galaxy redshift surveys. An accurate calibration of velocity bias will improve the usage of small-scale clustering information to constrain cosmological parameters (e.g, Wu & Huterer 2013; Zu & Weinberg 2013).

REFERENCES

Andreon S., Hurn M. A., 2010, MNRAS, 404, 1922
Becker M. R., McKay T. A., Koester B., et al., 2007, ApJ, 669, 905
Behroozi P. S., Wechsler R. H., Wu H.-Y., 2013a, ApJ, 762, 109
Behroozi P. S., Wechsler R. H., Wu H.-Y., Busha M. T., Klypin A. A., Primack J. R., 2013b, ApJ, 763, 18
Biviano A., Murante G., Borgani S., Diaferio A., Dolag K., Girardi M., 2006, A&A, 456, 23
Boylan-Kolchin M., Ma C.-P., Quataert E., 2008, MNRAS, 383, 93
Bryan G. L., Norman M. L., 1998, ApJ, 495, 80
Budzynski J. M., Koposov S. E., McCarthy I. G., McGee S. L., Belokurov V., 2012, MNRAS, 423, 104
Carlberg R. G., 1994, ApJ, 433, 468
Carlberg R. G., Couchman H. M. P., Thomas P. A., 1990, ApJL, 352, L29
Carlberg R. G., Yee H. K. C., Ellingson E., et al., 1997, ApJL, 476, L7
Cohn J. D., 2012, MNRAS, 419, 1017
Cohn J. D., Evrard A. E., White M., Croton D., Ellingson E., 2007, MNRAS, 382, 1738
Cole S., Lacey C., 1996, MNRAS, 281, 716
Colín P., Klypin A. A., Kravtsov A. V., 2000, ApJ, 539, 561
Conroy C., Wechsler R. H., Kravtsov A. V., 2006, ApJ, 647, 201
Danese L., de Zotti G., di Tullio G., 1980, A&A, 82, 322
Diaferio A., 1999, MNRAS, 309, 610
Diaferio A., Geller M. J., 1997, ApJ, 481, 633
Diemand J., Moore B., Stadel J., 2004, MNRAS, 352, 535 (D04)
Diemer B., Kravtsov A. V., More S., 2013, arXiv:1306.3165
Dolag K., Borgani S., Murante G., Springel V., 2009, MNRAS, 399, 497
Dubois Y., Devriendt J., Teyssier R., Slyz A., 2011, MNRAS, 417, 1853
Ellis R., Takada M., Aihara H., et al., 2012, arXiv:1206.0737
Evrard A. E., Bialek J., Busha M., et al., 2008, ApJ, 672, 122
Evrard A. E., Summers F. J., Davis M., 1994, ApJ, 422, 11
Faltenbacher A., Diemand J., 2006, MNRAS, 369, 1698 (F06)
Faltenbacher A., Kravtsov A. V., Nagai D., Gottlöber S., 2005, MNRAS, 358, 139
Frenk C. S., Evrard A. E., White S. D. M., Summers F. J., 1996, ApJ, 472, 460
Gao L., De Lucia G., White S. D. M., Jenkins A., 2004, MNRAS, 352, L1
Ghigna S., Moore B., Governato F., Lake G., Quinn T., Stadel J., 2000, ApJ, 544, 616
Gifford D., Miller C., Kern N., 2013, ApJ, 773, 116
Gifford D., Miller C. J., 2013, ApJL, 768, L32
Gill S. P. D., Knebe A., Gibson B. K., Dopita M. A., 2004, MNRAS, 351, 410
Girardi M., Biviano A., Giuricin G., Mardirossian F., Mezzetti M., 1993, ApJ, 404, 38
Goto T., 2005, MNRAS, 359, 1415

Gunn J. E., Gott III J. R., 1972, ApJ, 176, 1

Hahn O., Abel T., 2011, MNRAS, 415, 2101

Heisler J., Tremaine S., Bahcall J. N., 1985, ApJ, 298, 8

Klypin A., Gottlöber S., Kravtsov A. V., Khokhlov A. M., 1999, ApJ, 516, 530

Komatsu E., et al., 2011, ApJS, 192, 18

Lau E. T., Nagai D., Kravtsov A. V., 2010, ApJ, 708, 1419

Laureijs R., Amiaux J., Arduini S., et al., 2011, arXiv:1110.3193

Łokas E. L., Mamon G. A., 2003, MNRAS, 343, 401

Lubin L. M., Bahcall N. A., 1993, ApJL, 415, L17

Ludlow A. D., Navarro J. F., Springel V., Jenkins A., Frenk C. S., Helmi A., 2009, ApJ, 692, 931

Mamon G. A., Biviano A., Boué G., 2013, MNRAS, 429, 3079

Mamon G. A., Biviano A., Murante G., 2010, A&A, 520, A30

Martizzi D., Teyssier R., Moore B., Wentz T., 2012, MN-RAS, 422, 3081

Mortonson M. J., Hu W., Huterer D., 2011, Phys. Rev. D, 83, 023015

Munari E., Biviano A., Borgani S., Murante G., Fabjan D., 2013, MNRAS, 430, 2638

Nagai D., Kravtsov A. V., 2005, ApJ, 618, 557

Navarro J. F., et al., 2010, MNRAS, 402, 21

Newman A. B., Treu T., Ellis R. S., et al., 2013, ApJ, 765, 24

Old L., Gray M. E., Pearce F. R., 2013, MNRAS, 434, 2606

Puchwein E., Bartelmann M., Dolag K., Meneghetti M., 2005, A&A, 442, 405

Rasia E., Tormen G., Moscardini L., 2004, MNRAS, 351, 237

Reddick R. M., Wechsler R. H., Tinker J. L., Behroozi P. S., 2013, ApJ, 771, 30

Remus R.-S., Burkert A., Dolag K., Johansson P. H., Naab T., Oser L., Thomas J., 2013, ApJ, 766, 71

Rines K., Geller M. J., Diaferio A., 2010, ApJL, 715, L180

Rines K., Geller M. J., Diaferio A., Kurtz M. J., 2013, ApJ, 767, 15

Sales L. V., Navarro J. F., Lambas D. G., White S. D. M., Croton D. J., 2007, MNRAS, 382, 1901

Saro A., Mohr J. J., Bazin G., Dolag K., 2013, ApJ, 772, 47

Sifón C., Menanteau F., Hasselfield M., et al., 2013, ApJ, 772, 25

Skielboe A., Wojtak R., Pedersen K., Rozo E., Rykoff E. S., 2012, ApJL, 758, L16

Springel V., 2005, MNRAS, 364, 1105

Springel V., White S. D. M., Tormen G., Kauffmann G., 2001, MNRAS, 328, 726

Summers F. J., Davis M., Evrard A. E., 1995, ApJ, 454, 1

Teyssier R., Moore B., Martizzi D., Dubois Y., Mayer L., 2011, MNRAS, 414, 195

Tinker J. L., 2007, MNRAS, 374, 477

Tinker J. L., George M. R., Leauthaud A., et al., 2012, ApJL, 755, L5

Weinberg D. H., Colombi S., Davé R., Katz N., 2008, ApJ, 678, 6

Wetzel A. R., Tinker J. L., Conroy C., van den Bosch F. C., 2013, MNRAS, 432, 336

Wetzel A. R., White M., 2010, MNRAS, 403, 1072

White M., Cohn J. D., Smit R., 2010, MNRAS, 408, 1818

Wojtak R., Łokas E. L., Mamon G. A., Gottlöber S., Prada F., Moles M., 2007, A&A, 466, 437

Wu H.-Y., Hahn O., Wechsler R. H., Behroozi P. S., Mao Y.-Y., 2013b, ApJ, 767, 23

Wu H.-Y., Hahn O., Wechsler R. H., Mao Y.-Y., Behroozi P. S., 2013a, ApJ, 763, 70

Wu H.-Y., Huterer D., 2013, MNRAS, 434, 2556

Wu H.-Y., Rozo E., Wechsler R. H., 2010, ApJ, 713, 1207

Yahil A., Vidal N. V., 1977, ApJ, 214, 347

Zhang Y.-Y., Andernach H., Caretta C. A., et al., 2011, A&A, 526, A105

Zu Y., Weinberg D. H., 2013, MNRAS, 431, 3319